Nano Energy 72 (2020) 104662

Contents lists available at ScienceDirect

Nano Energy

journal homepage: http://www.elsevier.com/locate/nanoen

Giant energy storage density in PVDF with internal stress engineered polar nanostructures

Xintong Ren [a], Nan Meng [a,**], Han Zhang [a,c], Jiyue Wu [a], Isaac Abrahams [b], Haixue Yan [a,c], Emiliano Bilotti [a,c], Michael John Reece [a,c,*]

[a] School of Engineering and Materials Science, Queen Mary University of London, Mile End Road, E1 4NS, London, UK
[b] School of Biological and Chemical Sciences, Queen Mary University of London, Mile End Road, E1 4NS, London, UK
[c] NPU-QMUL Joint Research Institute of Advanced Materials and Structure (JRI-AMAS), Northwestern Polytechnical University, 710072, Xi'an, China

ARTICLE INFO

Keywords:
Energy storage
Ferroelectric relaxor
PVDF
Polar nanostructure
Internal stress
Ferrelectric switching

ABSTRACT

High power dielectric capacitors with high energy density are needed in order to develop modern electronic and electrical systems, including hybrid vehicles, telecommunication infrastructures and portable electronic devices. Relaxor ferroelectric polymers (RFP) are considered to be the most promising candidates for the next generation of capacitors owing to their relatively high energy storage density. However, the commercialization of RFP capacitors in power systems is hindered by their high cost and low dielectric breakdown strength. In this study, inexpensive, free-standing nano-crystalline (~3.3 nm) poly (vinylidene fluoride) (PVDF) films with high β phase content (~98%), "relaxor-like" ferroelectric behaviour and high breakdown strength (880 kV/mm) were fabricated using the facile Press & Folding (P&F) technique. An internal stress dominated polarization switching model is proposed to explain the origin of the relaxor-like ferroelectric behaviour. The internal stress generated during pressing alters the intermolecular chain distance of the (200) plane of β-PVDF from 4.24 Å in internal stress free films to 4.54 Å in P&F films, corresponding to a tensile strain and residual stress of 7.11% and 142 MPa, respectively. The internal stress acts to partially reverse the polarization on reversal of the applied electric field. This, combined with preferred in-plane orientation of the crystallites, results in a polar nanostructure with high polarization reversibility at high electric fields. A giant discharged energy storage density of 39.8 J/cm^3 at 880 kV/mm was achieved for P&F films, which surpasses all previously reported polymer-based materials.

1. Introduction

Among all of the energy storage methods, dielectric capacitors excel in terms of stability, ultrahigh power density (up to 10^8 W/kg) and fast charging-discharging speed (~10 ns – 1 ms). They have great potential in advanced electronic and electrical systems, wearable devices, medical apparatus and electric vehicles [1].

Compared with traditional inorganic-based bulk ceramics, flexible polymer-based dielectric materials have drawn considerable attention owing to their high breakdown strength, superior mechanical properties and good processability [2]. However, the discharged energy density (U_e) of polymer dielectric capacitors (1–2 J/cm^3) is much lower than batteries (200–2500 J/cm^3) and supercapacitors (20–29 J/cm^3), limiting them from achieving miniaturization to fulfil the requirements for modern energy storage systems [3–7].

During the last few decades, great effort has been dedicated to the study of poly (vinylidene fluoride) (PVDF), a highly polarizable ferroelectric polymer with a large dipole (pointing from the fluorine atoms to the hydrogen atoms), for dielectric energy storage applications [8,9]. PVDF exhibits a high relative permittivity ε_r of ~10–12 (1 kHz) and high field-induced polarization P_{in} (~0.10 C/m^2) at high applied electric fields (~200 kV/mm) due to the non-polar α phase to polar δ phase transition at 170 kV/mm, followed by the β phase transition at 500 kV/mm [10,11]. PVDF has a high remnant polarization P_r produced by ferroelectric switching, which severely decreases its charge-discharge efficiency and restricts it from achieving high U_e [12]. To overcome these barriers, methods for producing relaxor ferroelectric behaviour with more reversible polar structures under high fields have been explored, including chemical modification (e.g. crosslinking [13,14], grafting [15,16], synthesis of PVDF-based copolymers and terpolymers

* Corresponding author. School of Engineering and Materials Science, Queen Mary University of London, Mile End Road, E1 4NS, London, UK.
** Corresponding author.
E-mail addresses: n.meng@qmul.ac.uk (N. Meng), m.j.reece@qmul.ac.uk (M.J. Reece).

https://doi.org/10.1016/j.nanoen.2020.104662
Received 13 January 2020; Received in revised form 21 February 2020; Accepted 29 February 2020
Available online 4 March 2020

etc. [17–20]), high-energy electron/γ-ray irradiation [21], polymer blending [22,23], nanocomposites [24–28] and multilayer structure design [29–31]. Utilising chemical reactions to modify the microstructure is an effective way to improve the functional properties. Particularly, incorporating bulk monomers, such as trifluoroethylene (TrFE), chlorofluoroethylene (CFE) and chlorotrifluoroethylene (CTFE), into the PVDF molecular chain to obtain P(VDF-TrFE-CFE) and P (VDF-TrFE-CTFE) terpolymers can break the large ferroelectric domains into polar nanodomains and broaden the interchain distance [17, 19]. Such a chemical route can successfully transform ferroelectric PVDF into a relaxor ferroelectric, displaying higher charge-discharge efficiency (50–70%) compared with pristine PVDF (40–50%) [17,32]. However, the synthesis of terpolymers involves complex chemical reactions and expensive equipment. Moreover, the dielectric breakdown strength E_b and mechanical properties of PVDF are seriously deteriorated. The Young's modulus decreases from 1.2 to 1.5 GPa for PVDF to 150 MPa for P(VDF-TrFE-CFE) because of defects and reduced crystallinity [24]. These hindrances have limited the use of terpolymers in practical applications. Alternative approaches, including designing PVDF-based polymer blends or nanocomposites, usually involves a compromise between high polarisability and high breakdown strength [22,24,33].

The microstructure and morphology of semi-crystalline polymers profoundly affects their energy storage capability, including different crystalline phases, crystallite size (or lamellae thickness l) and preferred chain orientation [34–36]. It is well accepted that small crystallite size is favourable for enhancing E_b and therefore achieving higher U_e [33,37]. Also, the orientation of the polymer chains plays a significant role in determining the polarisability of PVDF. A higher ε_r of 12–13 is observed in PVDF when its chains (c-axis) are perpendicularly aligned to the applied electric field compared with when the molecular chains are parallel with the applied electric field (ε_r: 5–6) as the dipoles can more easily follow the field when they are randomly distributed in the plane parallel to the field [36,38]. Compared with non-polar α-PVDF, the electroactive β and γ phases are more desirable because of their higher P_{in} at the same field. According to the literature, for virgin PVDF homopolymers, the γ phase with T_3GT_3G' chain conformation exhibits a higher breakdown strength E_b of 500 kV/mm and U_e of 14 J/cm^3 than the β phase since the early polarization saturation in the β phase is avoided [34,39].

In this paper, relaxor-like ferroelectric behaviour was achieved by producing internal stress engineered polar nanostructures in PVDF films prepared using the facile and scalable P&F processing technique. The Press & Folding (P&F) method produces ultrahigh β phase content and reduced crystallite size (~4 nm) in a laminated structure [40]. In this paper, we report the mechanism by which P&F produces relaxor-like ferroelectric behaviour in PVDF, and use this knowledge to optimise its energy storage properties. The internal lattice stresses are produced during the fabrication of the films. They broaden the interchain distance in the crystalline phase and drive the reverse switching of the dipoles on removal of the applied electric field, leading to relaxor-like ferroelectric behaviour and an outstanding energy storage density (39.8 J/cm^3 at 880 kV/mm). It is well known that mechanical drawing can have a profound impact on the structure and properties of thermoplastic polymers, from their mechanical properties to thermal conductivity [41–44]. To the best of our knowledge, this is the first time that high internal stress (up to ~142 MPa) has been employed to engineer polar nanostructures with ultrahigh reversibility under high electric fields. Herein, we demonstrate that internal stress build-up is the dominant factor in achieving a record high energy density.

2. Experiment and methods

2.1. Materials

Polyvinylidene fluoride (PVDF) homopolymer powder with high molecular weight M_w of 670–700 kg/mol (Solef®6020) was purchased from Solvay. Rocol® 400 ml PTFE Mould Release Agent Plastic was purchased from RS Components UK. All of the materials were used as received.

2.2. Film fabrication and processing

Hot-pressed film: 4.0 g of PVDF powder was weighed using an analytical balance (OHAUS Explorer, USA) and placed between two aluminium sheets. The initial hot-pressed PVDF films were prepared using a Dr. Collin hot press machine P300E (Dr. COLLIN GmbH, Germany) at 180 °C and 150 kN for 5 minutes, followed by water cooling to 50 °C under constant pressure. A round film with a diameter of ~10 cm (final pressure ~20 MPa) and a thickness of ~250–350 μm was obtained.

Press & folding (P&F) films: As illustrated in Fig. 1a, to facilitate the exfoliation of single layers of the P&F films to enable high field characterisation of the materials, the PTFE mould release agent was sprayed onto the surface of the films before each P&F cycle. This did not affect the structures and properties of the films. The hot-pressed films were first folded in half and then pressed at 300 kN (initial pressure ~76 MPa) and 50 °C. The temperature was then increased to 165 °C and maintained for 10 minutes under constant pressure. Finally, the film was water cooled to 50 °C under constant pressure. Different P&F protocols were used to investigate the mechanisms involved in the P&F process (eg. pressure loading & unloading sequence, P&F temperature). All of the films were P&F for 6 cycles, after which a single layer film of ~10–20 μm thickness could easily be exfoliated for further characterisation.

2.3. Characterisation

Microstructures: The cross-section morphology of the films were studied using a scanning electron microscopy (SEM) (FEI Inspect-F, USA) after quenching in liquid nitrogen and then fracturing them. A Fourier transform infrared spectrometer (FTIR) Tensor 27 with ATR mode (Bruker Optik GmbH, Germany) was used to determine the chain conformations and crystalline phases. The relative fraction of β phase content in films containing both α and β phases were calculated using equation (1), derived using the Lambert-Beer Law, where A_α and A_β are the absolute intensities of the peaks at 762 cm^{-1} and 840 cm^{-1}, respectively [45].

$$F(\beta) = \frac{A_\beta}{1.26A_\alpha + A_\beta} \quad (1)$$

Raman spectra between 1500 and 100 cm^{-1} were measured using a Renishaw inVia™ Raman microscope with a 785 nm laser, 1200 lines mm^{-1} grating and 50 × objective lens (Renishaw, UK) to investigate the internal strain.

X-ray diffraction (XRD) patterns were acquired using an Xpert-Pro diffractometer (PANalytical, Netherlands) with Cu-Kα radiation (wavelength $\lambda = 0.15418$ nm) with a 2θ range of 5°–70° to study the crystalline structure and internal stress. The average crystallite size was estimated according to Scherrer's equation (equation (2)),

$$D_{hkl} = \frac{K\lambda}{\beta_{hkl}\cos\theta} \quad (2)$$

in which D_{hkl} is the average crystallite size along the (110)/(200)$_\beta$ crystal plane, K is the shape factor which varies with the crystallite shape (0.89 was chosen in this case), λ is the wavelength of the incident X-rays, β_{hkl} is the full width at half maximum of the (110)/(200)$_\beta$ reflection, θ is the diffraction angle. The interchain distance is given by Bragg's law (equation (3)),

$$\lambda = 2d_{hkl}\sin\theta_{hkl} \quad (3)$$

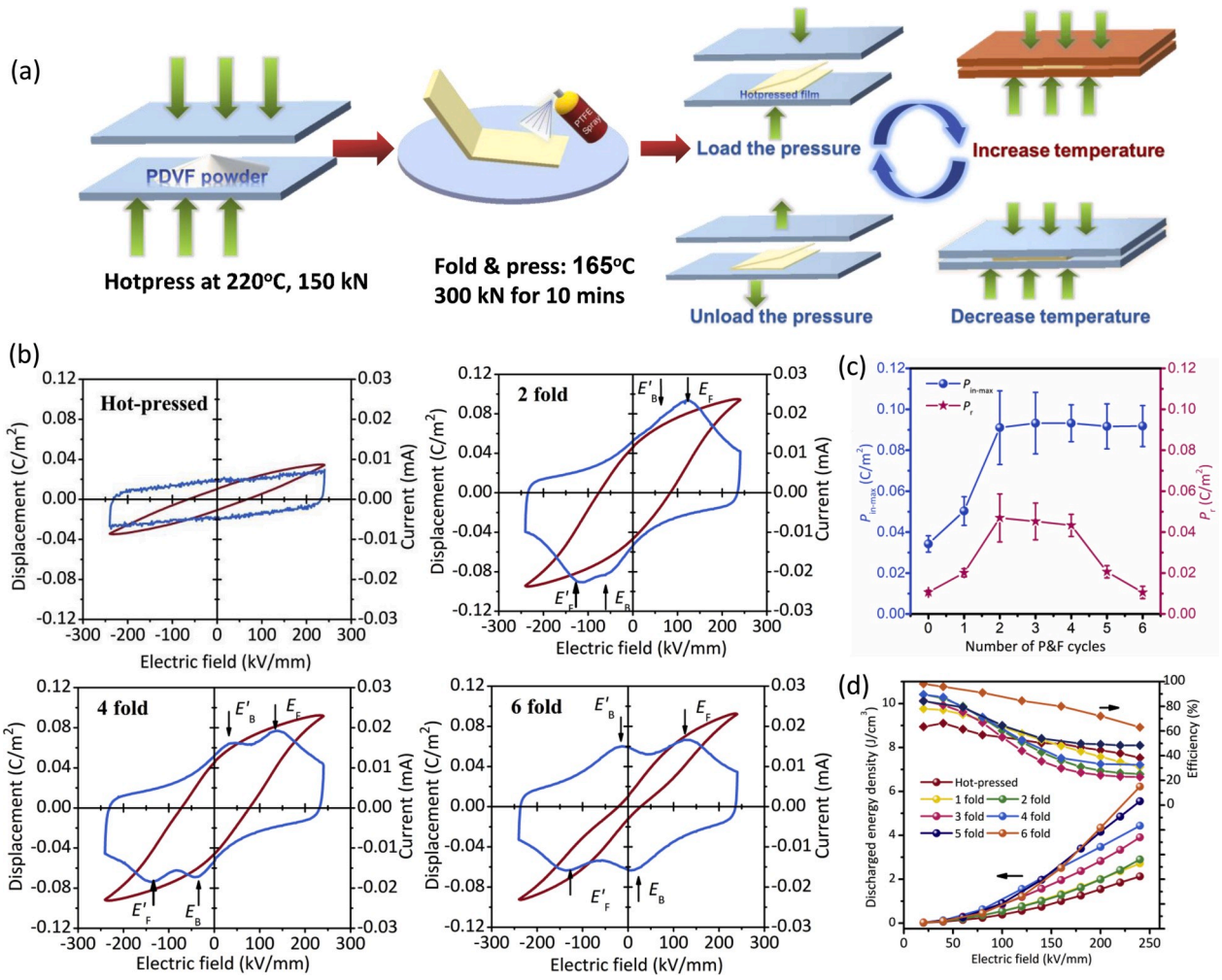

Fig. 1. (a) Schematic demonstration of P&F procedure with PTFE releasing agent sprayed on the surface. (b) *I-E* and *D-E* loops at 240 kV/mm for hot-pressed PVDF film and P&F PVDF films after 2, 4 and 6 cycles. Comparison of hot-pressed PVDF film and 165 °C P&F PVDF films after 1 to 6 cycles: (c) P_r, $P_{in\text{-}max}$ at 240 kV/mm; (d) Discharged energy density and charge-discharge efficiency.

The internal lattice strain ε inside the P&F films was evaluated by the change of interchain distance obtained from the XRD data using equation (4), in which d_0 of 4.24 Å is the β phase interchain distance of annealed films without internal strain (peak position at 20.95°), while d_1 is the interchain distance of the P&F films. The tensile mechanical properties of hot-pressed PVDF films and 1-fold to 5-fold PVDF films prepared at 165 °C were measured using an Instron 5566 tensile tester (Instron, USA) with a drawing speed of 20 mm/min at room temperature (Fig. S1). The 6-fold films were not measured because of their limited sample size. The associated local internal stress σ_r was approximately evaluated assuming linear-elastic behaviour and using equation (5), where ε is the lattice strain and K is the bulk modulus. In this case, a Young's modulus E of ~1800 MPa, estimated from the mechanical test results (Fig. S1), was used to calculate the bulk modulus K. The bulk modulus was calculated using equation (6) and the Poisson's ratio ν (0.35) was obtained from the literature [46].

$$\varepsilon = \frac{d_1 - d_0}{d_0} \tag{4}$$

$$\sigma_r = \varepsilon K \tag{5}$$

$$K = \frac{E}{3(1-2\nu)} \tag{6}$$

Two-dimensional wide-angle X-ray diffraction (2D-WAXD) ring patterns of the surface and cross-section of the films were obtained using transmission and reflection modes of single crystal X-ray diffractometer with a molybdenum (Mo) target (λ = 0.7107Å, Kappa ApexII Duo, Bruker AXS GmbH, Germany).

Electrical properties: The dielectric properties versus frequency from 100 Hz to 100 MHz were measured using a Precision Impedance Analyzer (Agilent 4294, USA) at room temperature. Bipolar and unipolar current - electric field (*I-E*) loops and electric displacement - electric field (*D-E*) loops were acquired using a ferroelectric hysteresis loop measurement system (National Physics Laboratory, UK) at room temperature and 10 Hz [47]. The maximum output voltage of the voltage amplifier is 10 kV. The discharged energy storage density was calculated by integrating the discharge curve of the *D-E* loops. The breakdown field was measured during the ferroelectric hysteresis loop testing and analysed using the two-parameter Weibull distribution:

$$P(E) = 1 - \exp[-(E/E_b)^{\beta}] \tag{7}$$

where the E is the experimentally measured breakdown field, E_b is the characteristic breakdown strength at which the probability of dielectric breakdown is 63.2%, $P(E)$ is the statistical cumulative probability of dielectric breakdown and β is the Weibull parameter related to the reliability of the films under electric fields. The analysis was based on 10 measurements for single layer PVDF films peeled off from 6-fold PVDF films prepared at each P&F temperature.

3. Results analysis

3.1. Electric properties and structure evolution during P&F

To obtain a comprehensive understanding of the mechanism behind the P&F process, the evolution of ferroelectric behaviour and structure with increasing P&F cycles are presented and analysed in this section.

3.1.1. Ferroelectric and energy storage properties

Fig. 1b shows the current - electric field (*I-E*) loops and electric displacement - electric field (*D-E*) loops for the hot-pressed PVDF films and P&F PVDF films prepared at 165 °C after 2, 4 and 6 folds. Due to the relatively large thickness of the initial hot-pressed films (typically 40–50 μm), which limited the application of very large electric fields with our set-up (maximum voltage 10 kV), all of the results were obtained at a relatively low electric field of 240 kV/mm to enable comparison. The field was still high enough to demonstrate the evolution of the ferroelectric properties. The pristine hot-pressed PVDF films behaved like linear dielectrics, with a maximum field-induced polarization $P_{in\text{-}max}$ of only 0.032 C/m^2, which is explained by their predominantly non-polar α phase content that requires a much higher applied electric field (500 kV/mm) to achieve the ferroelectric β phase transformation [48]. After P&F twice, a broad current peak was observed in the 1st quadrant of the *I-E* loops, which was actually composed of two peaks, which are more distinct in the 3rd quadrant. These four peaks, denoted as E_F, E'_F, E_B, and E'_B (F: forward poling; B: backward poling), indicate that reversible polar structures started to appear in the P&F films. These polar structures were switched by the applied electric field and partially reversed back when the external field direction was reversed. The pair of current peaks were more distinct in the 3rd quadrant because the initial applied field led to the equilibration of the polar structures. The four peaks became more evident and separated

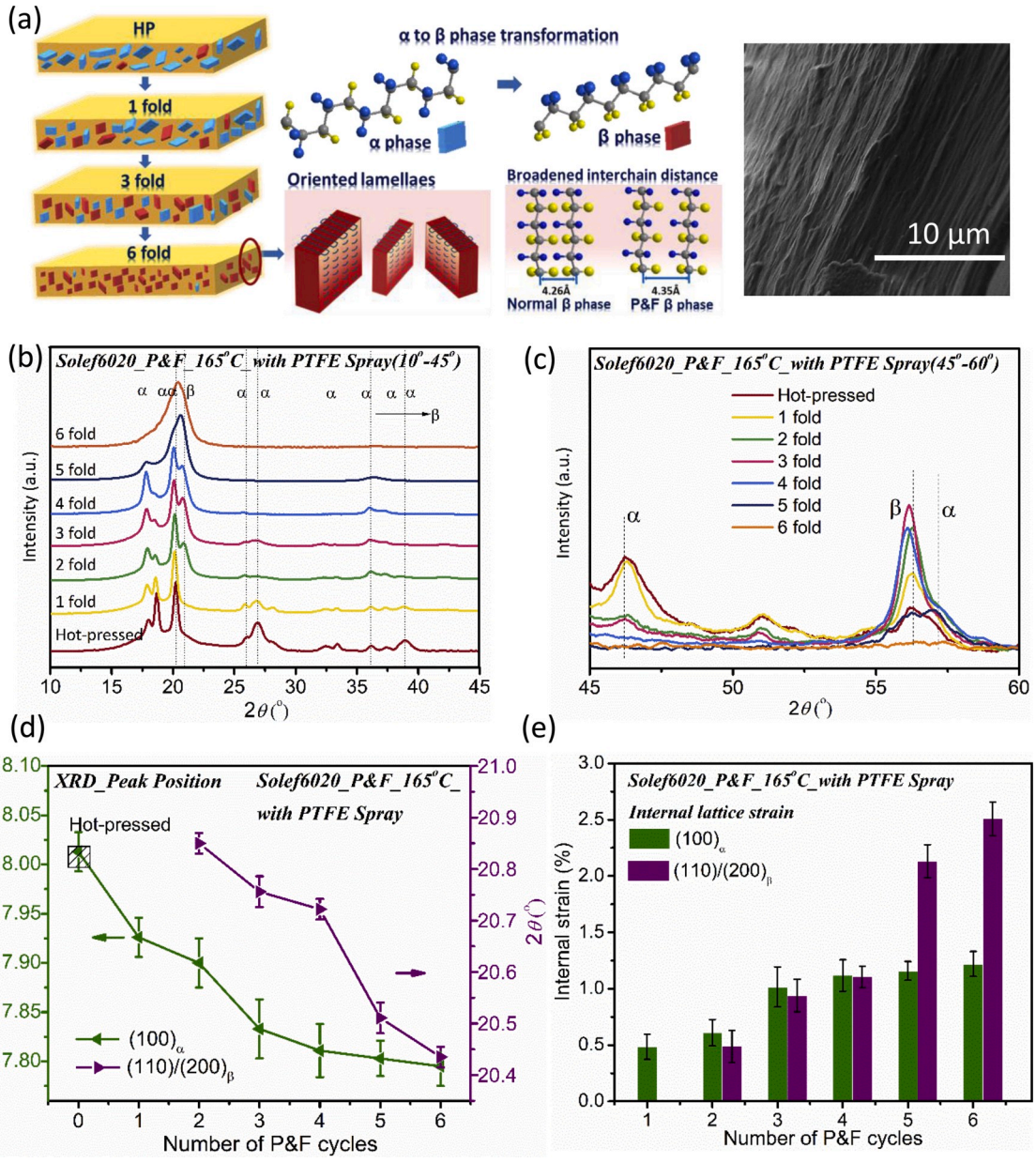

Fig. 2. (a) Schematic diagram of PVDF structure change with increasing P&F cycles, including α to β phase transformation, reduced crystallite size, induced preferred orientation and broadened interchain distance resulting from the accumulated internal tensile stress. SEM image of the cross-section of a 6-fold PVDF film. XRD patterns from (b) 10° to 45° 2θ and (c) from 45° to 60° 2θ (enlarged); (d) XRD diffraction peak positions; (e) Internal lattice strain of hot-pressed PVDF film and 165 °C press-folded PVDF films after 1 to 6 P&F cycles.

after 4 P&F cycles. Further P&F cycles enhanced the reversibility of the polar structures as the E_B and E'_B peaks moved to the 2nd and 4th quadrants respectively, suggesting that the reversal of the polar structures became easier (Fig. S2). With the appearance of four peaks in the *I-E* loops, the remnant polarization P_r was significantly reduced from 0.048 to 0.009 C/m^2 with increasing P&F cycles from 2 to 6, and the *D-E* loops transformed from typical ferroelectric hysteresis loops to "relaxor-like" ferroelectric loops. Meanwhile, the $P_{in\text{-}max}$ maintained a similar value after six folds, which is favourable for achieving a high discharged energy density and high efficiency since the U_e is generally determined by the difference between $P_{in\text{-}max}$ and P_r as well as the applied electric field. As a result, the PVDF films after six folds exhibited a U_e of 6.3 J/cm^3 with an efficiency of 63% compared to the pristine hot-pressed films of 2.2 J/cm^3 and 38%, respectively.

3.1.2. Structure evolution

It is very likely that the development of relaxor-like ferroelectric behaviour in the P&F PVDF films is strongly dependent on their structure evolution during the P&F process, as schematically illustrated in Fig. 2a. The FTIR spectra in Fig. S3a and the Raman spectra in Fig. S3c show that P&F produced a phase transformation from the α to β phase during the compression step. After press-folding for 6 cycles, the β phase content was remarkably enhanced from 8% in the hot-pressed PVDF to ~98%, as calculated using the FTIR spectra. The XRD results give us further information on crystallite size, preferred orientation of the polymer chains and lattice structures (Fig. 2b–e). The crystallite size, determined from peak broadening, decreased from ~17.5 nm to ~5.0 nm for the α phase and from 12.4 nm to 4.6 nm for the β phase with increasing number of P&F cycles (Fig. S3b), which is attributed to increasing effective applied stress with increasing number of P&F cycles. Moreover, the constraining effect originating from the folded multilayer structure and quenching under pressure also favour small crystallites by limiting their growth.

Both of the XRD peaks belonging to the $(110)/(200)_\beta$ crystal planes at 20.95° 2θ and the peak belonging to the $(100)_\alpha$ crystal plane at 18.02° 2θ in the internal strain free PVDF continuously shifted toward lower angles (20.44° 2θ and 17.79° 2θ after P&F 6 cycles, respectively) with increasing P&F cycles (Fig. 2c and d). This corresponds to an internal tensile strain of 2.45% in the β-PVDF crystallites, which corresponds to an internal stress of ~49 MPa (Fig. 2e). During unloading, the polymer mechanically relaxed and a residual tensile internal stress was generated in the crystallites in the direction perpendicular to the film surface. This will be discussed in more detail in the next section. To further confirm the existence of internal strain, the Raman spectra of the PVDF films with different P&F cycles were acquired and the peak at 1057.1 cm^{-1}, attributed to the in-plane symmetric stretching of the C–C bonds in the α-phase, was selected to reveal the effect of internal stress (Figs. S3c–d). Similar to the XRD peak shift, the Raman peak also experienced an obvious shift from 1057.1 cm^{-1} to 1059.0 cm^{-1} as the internal stress stretched and constrained the C–C bond, requiring higher energy to activate these molecular vibrations [49].

The applied stress induced preferred in-plane orientation of the polymer chains, as evidenced by the disappearance of the β phase diffraction peaks at 36.62° and 56.21° 2θ after 6 P&F cycles, which belong to the $(020)/(310)_\beta$ and $(221)_\beta$ crystal planes, respectively (Fig. 2b). To facilitate comparison, the XRD patterns between 45° and 60° 2θ are enlarged in Fig. 2c. The intensity of the $(221)_\beta$ peak at 56.21° 2θ first increased, reaching a maximum as the P&F cycles increased to three, which is ascribed to the increased β phase content of the P&F films. Then, it started to decrease and broaden with further P&F cycles and eventually vanished. This is consistent with the oriented lamellae morphology observed in the cross-section of the PVDF films after P&F 6 cycles (Fig. 2a) and the 2D-WAXD split ring patterns shown in Fig. 3a. As calculated from the unit cell parameters of β-PVDF ($a = \sqrt{3}b$, $a = 8.56$ Å, $b = 4.91$ Å, $c = 2.56$ Å), the inner ring with four arcs exhibiting angles of 60°/120° indicate that the *b*-axis of the unit cell tended to align parallel to the film surface, while the *a*-axis was more likely to be out of the film plane. This is consistent with the reported results for biaxially oriented polytrifluoroethylene (PTrFE) [50] and β-PVDF [51] prepared by rolling with a draw ration of 5, which also exhibit the same preferred orientation with polar *b*-axis oriented in-plane. Herein, a polarization switching model dominated by internal stress is proposed based on the preferred orientation of the crystallites in the press-folded PVDF films and the nπ/3 collective rotation model [52,53]. As shown in Fig. 3a, the dipoles in these well-aligned edge-on lamellaes are parallel to the film surface in the pristine film before poling. Distinctive stages are observed upon applying and removing the high external field (Fig. 3b). These in-plane dipoles are switched with a ±60° rotation upon applying high fields ($|E| > |E_F|$ or $|E'_F|$) and are reversed back to the in-plane state by the high internal stresses when the external field is withdrawn. Therefore, the internal strain not only stretched the polymer chain and expanded the intermolecular chain distance but also acted as the driving force to reverse the electric field switched dipoles back to their original states, leading to a dramatically reduced P_r and relaxor-like ferroelectric behaviour in the 6 fold P&F films.

Annealing at high temperature without pressure was carried out at 165 °C for 12 h to release the internal stress and reveal its influences on the ferroelectric properties. The XRD pattern of a 6-fold P&F PVDF film before and after annealing at 165 °C for 12 h are shown in Fig. 4a. The β phase peak at 20.44° 2θ in the P&F PVDF shifted back to 20.95° 2θ, and the peaks representing the α phase became prominent in the XRD pattern. As calculated from the fitted results, the α phase accounted for 26% of the crystalline phase and the average size of the β phase crystallites increased from 4.6 nm to 7.5 nm. It is also notable that the $(020/310)_\beta$ peak reappeared. This suggests that during the annealing the crystallites were free to rotate about their chains and the preferred orientation of the crystallites was lost. The *D-E* and *I-E* loops of the annealed samples (Fig. 4b) show higher P_r and the four current peaks merged into two at high fields. It is therefore clear that the ferroelectric behaviour of the P&F films is strongly dependent on the high internal stress in the films.

3.2. Understanding the origin of internal stress in P&F PVDF films

It is necessary to understand the origin of the internal strain in P&F films in order to further improve their ferroelectric and dielectric properties, and energy storage density. The processing steps determine the final structure and properties of the P&F films. In this section the main factors influencing the internal stress and structure are explored.

3.2.1. Loading & unloading sequence

Three different P&F procedures with different loading & unloading sequences were carried out in order to understand the importance of the different conditions (Fig. 5a). Firstly, the initial hot-pressed film was P&F using the normal P&F procedure as described in the experimental details (denoted by "***PT***"). A second set of films were prepared with the "***TP***" procedure, in which the temperature was increased first and then the pressure was applied and maintained until the sample was cooled to 50 °C. The last batch of samples were heated and cooled without pressure (denoted as "***TP-CWP***").

FTIR and XRD measurements were performed to reveal any differences in the structure of the P&F films fabricated using the three different P&F procedures. A comparison of the fraction of β phase calculated using the Lambert-Beer Law from the FTIR data (Fig. S4) is shown in Fig. 5b. After 6 P&F cycles, both the "***PT***" and "***TP***" films contained more than 95% β phase in the crystalline phase, while the "***TP-CWP***" film exhibited a slightly lower β phase content (90%). Since FTIR only provides information on the local chain conformation, it is necessary to double check the XRD results to confirm the crystalline composition. As shown in Fig. 5c, the 6-fold "***PT***" and "***TP***" films displayed similar XRD patterns, meaning that the order of the application of pressure and temperature did not make a difference to the final

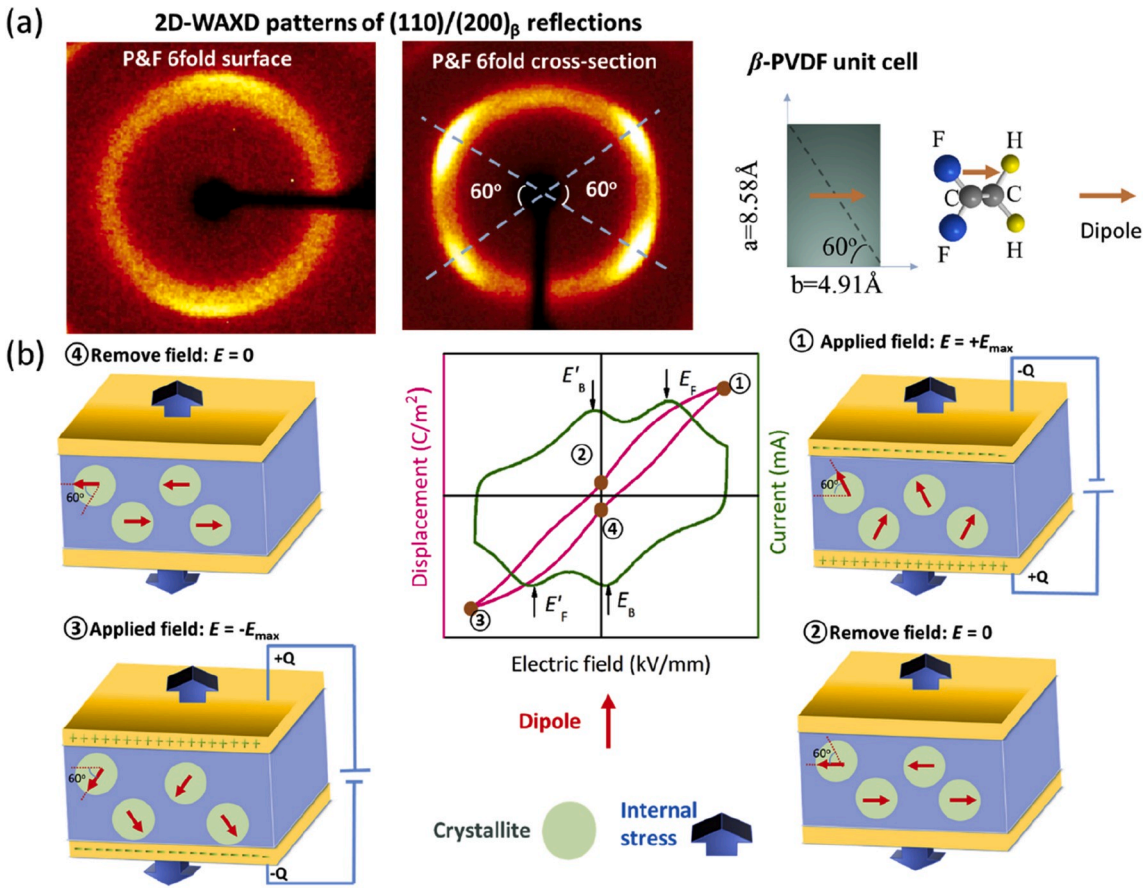

Fig. 3. (a) 2D-WAXD patterns for the surface (data collected using transmission mode) and the cross-section (data collected using reflection mode) of the 6-fold PVDF film prepared at 165 °C, and the schematic diagram of the *β*-PVDF unit cell and lamellae with *b*-axis in-plane. (b) Schematics of the internal-stress dominated polarization switching model for the press-folded PVDF with relaxor-like behaviour.

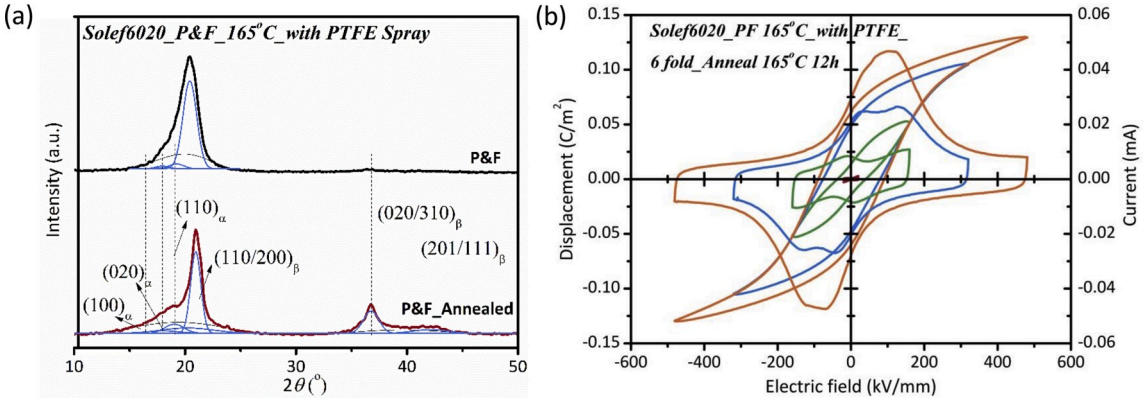

Fig. 4. Comparison of pristine 6-fold P&F films and P&F films annealed at 165 °C for 12 h: (a) XRD patterns; (b) *D-E* and *I-E* loops with incrementally increasing maximum electric fields.

structure during P&F. However, the 6-fold film, prepared using the "***TP-CWP***" procedure exhibited notable α phase peaks at 17.97°, 18.67° and 20.05° 2*θ* (fitted pattern is shown in Fig. S5) compared to the films fabricated using the "***PT***" and "***TP***" procedures, indicating that an amount of *α* phase reappeared (~21% as calculated from the fitted XRD pattern) during pressureless cooling. Also, the *β* phase peak shifted back to 20.90° 2*θ* and the peaks at high diffraction angles appeared again, suggesting that the internal stress in the "***TP-CWP***" P&F film was much lower than in the films cooled under pressure and the preferred orientation of the *β* phase crystallites was lost during the "cooling without pressure" step. These results are indicative of the significance of the "pressure unloading" step. Holding at 165 °C and high pressure for 10 minutes resulted in the build-up of internal stresses, preferred orientation and reduced crystallite size, as previously demonstrated. These changes were stabilized and constrained during cooling by maintaining the high pressure. Without high pressure during cooling, the residual stress is reduced, resulting in the disappearance of the reversible polar nanostructures, which is confirmed by the merging of the current peaks in the *I-E* loops and the high P_r of 0.049 C/m^2 compared to 0.009 C/m^2 for the 6-fold film prepared using the **"*PT*"** procedure at the same

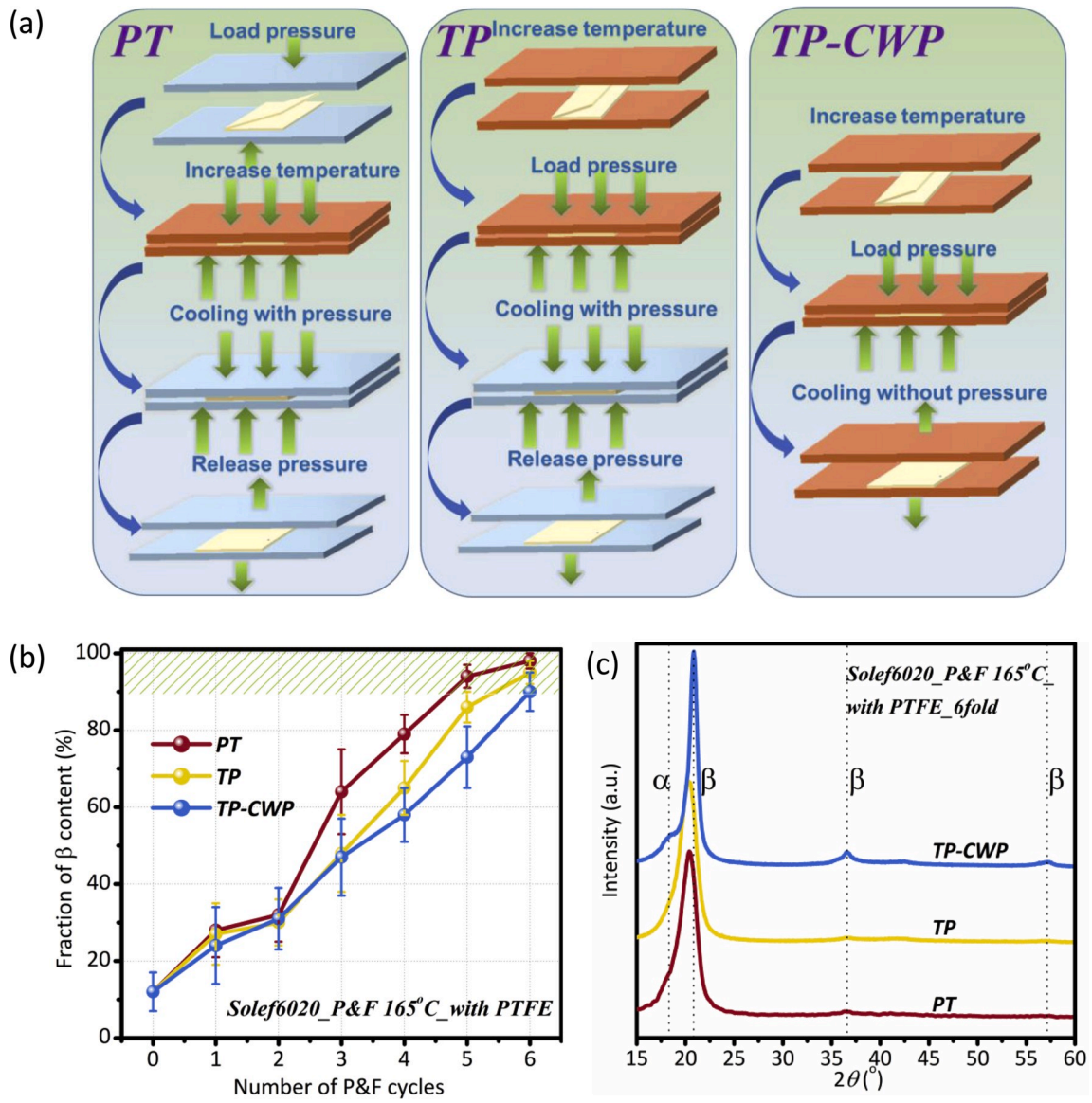

Fig. 5. (a) Schematic illustrating the three different P&F protocols: **"*PT*"**, **"*TP*"** and **"*TP-CWP*"**. (b) Evolution of β phase content with increasing P&F cycles for the three different processing procedures using the FTIR data in Fig. S4. (c) XRD patterns comparison of P&F films using the **"*PT*"**, **"*TP*"** and **"*TP-CWP*"** procedures respectively.

applied field of 240 kV/mm (Fig. S6).

3.2.2. *Press & folding temperature*

Based on the previous results, it is clear that applied pressure is crucial for achieving and maintaining the favourable microstructures and properties of the P&F films. In order to obtain higher internal stress in the P&F films, lower P&F temperatures were applied to reduce the mobility of the polymer chains and enhance the constraining effect during the PT procedure. As revealed by the FTIR results (Fig. S7), all of the P&F films processed from 60 °C to 165 °C experienced an α to β phase transformation, with a ~98% β phase content in all of the 6-fold films. However, there was a large variation in crystallite size and internal stress, as evidenced by the peak broadening and shift in the XRD patterns in Fig. 6a–c. The average crystallite size reduced from 4.6 nm to 3.3 nm by lowering the P&F temperature from 165 °C to 60 °C. The β phase peak at 20.95° 2θ in annealed films monotonically shifted from 20.44° 2θ in the 165 °C P&F film to 19.54° 2θ in the 60 °C P&F film, as a result of a higher internal stress induced at the lower temperature. The interchain distance of the β phase increased from 4.34 Å to 4.54 Å (compared to 4.24 Å for annealed films with no internal stress) with increasing internal stress, leading to higher reversibility of the polar nanostructure.

As seen in Fig. 6c, the internal strain in the 6-fold film P&F at 60 °C was ~7.11%, nearly 3 times higher than in the 165 °C P&F film. The estimated internal stress was ~142 MPa in the 6-fold film P&F prepared at 60 °C compared to 49 MPa for the film P&F at 165 °C. Therefore, it can be concluded that conducting P&F at lower temperatures enhanced the work hardening and constraining effect between the film layers to induce higher internal strain during P&F. Consequently, polar nanostructures with higher reversibility and higher U_e were achieved in films P&F at lower temperatures.

3.3. *Reversible polar nanostructure and enhanced energy storage property*

To understand the origin of the reversible polar nanostructure of the P&F films, the frequency dependence of the low-field dielectric properties of the 6-fold P&F films prepared at different temperatures, before and after *D-E* measurement (400 kV/mm), are shown in Fig. 7a and b.

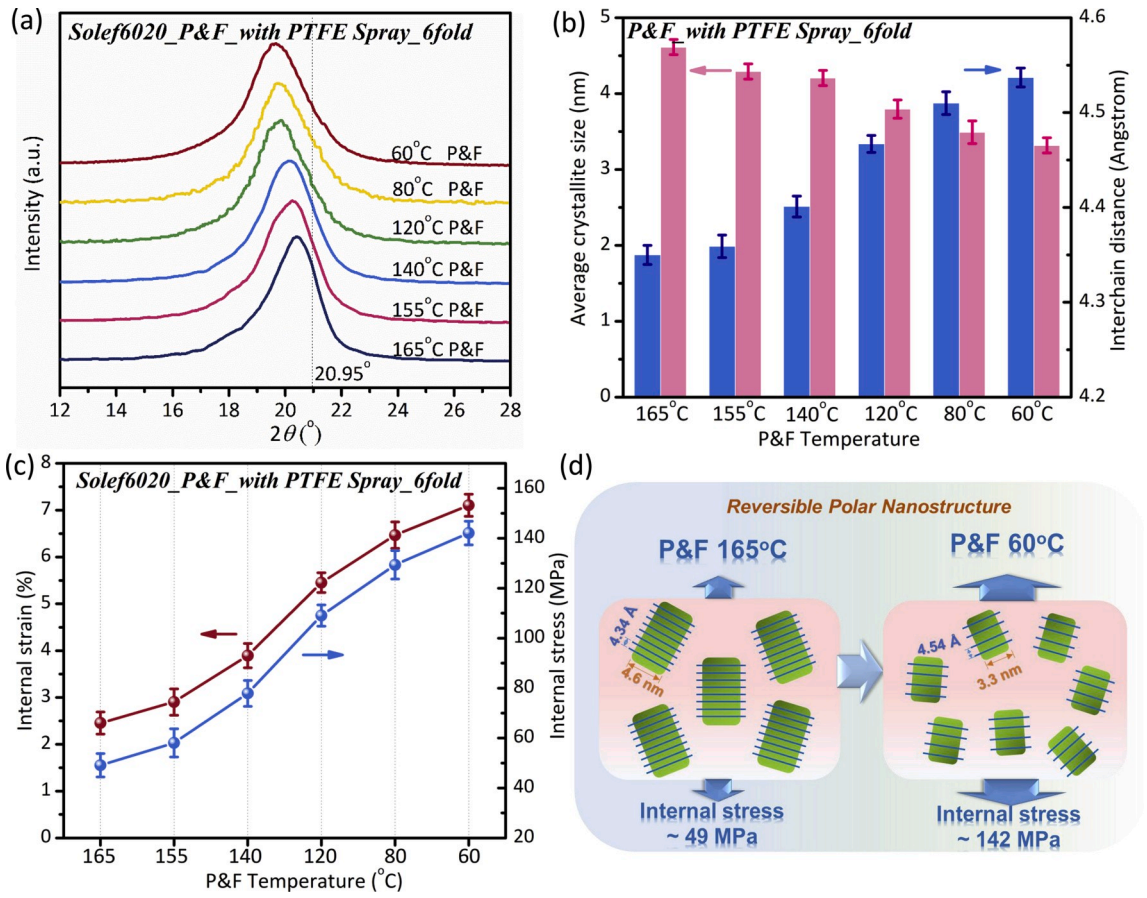

Fig. 6. Comparison of 6-fold P&F films prepared at temperatures from 60 °C to 165 °C: (a) XRD patterns; (b) average crystallite size and interchain distance; (c) internal local strain and internal stress. (d) Schematic of the structure evolution including internal tensile stress, crystallite size and interchain distance as a function of temperature.

Both before and after poling at high fields, the P&F films prepared at lower temperatures showed higher dielectric constant over the entire frequency range. After the *D-E* measurement, the dielectric constant of all of the P&F films prepared at all of the temperatures experienced an increase. These observations can be explained by the preferred orientation of the films produced by P&F and poling (Fig. 3).

For non-linear dielectrics, such as ferroelectric materials, the relationship $\varepsilon_r = (\partial D/\partial E)/\varepsilon_0$ is invalid because the change of electric displacement D produced by an applied field have an extrinsic contribution from domain wall movement and are not perfectly reversible. Nevertheless, the electric displacement D is closely related to the dielectric constant ε_r at high fields, after saturation of the polar switching. The $(\partial D/\partial E)/\varepsilon_0$ term has been used to qualitatively correlate the high field dielectric constant ε_r as a function of electric field by several research groups [37,54]. Similarly, the derivative of D with respect to E for the charging process at different electric fields for P&F films prepared at 60 °C, 80 °C, 140 °C and 165 °C are plotted in Fig. 7c–f, along with their corresponding unipolar *D-E* loops. All of the derivative curves exhibited a peak, at which the greatest rate of polarization associated with dipole switching occurred. The intensity of the peak is related to how easily the dipoles could be aligned by the electric field and the number of contributing dipoles. The peak position corresponding to the *D-E* loops produced with an electric field amplitude of 640 kV/mm shifted from 129 kV/mm to 115 kV/mm as the P&F temperature decreased from 165 °C to 60 °C, suggesting that the dipoles in the film P&F prepared at lower temperatures were easier to orient with the electric field. The magnitude of the peak for P&F films prepared at 165 °C decreased with increasing applied field amplitude, indicating that a proportion of the polar nanostructure aligned by the electric field did not switch back to their initial state during the discharging process. On the contrary, the maximum $(\partial D/\partial E)/\varepsilon_0$ value was stable at high field in the 60 °C P&F films which exhibits higher internal stress, as the stress can reverse the polar nanostructure back to in-plane orientation upon removal of the external field.

The P&F film prepared at 60 °C had a more reversible polar structure, resulting in a higher $P_{in\text{-}max}$ of 0.129 C/m^2 and a higher U_e of 26.6 J/cm^3 at 640 kV/mm compared with the P&F film prepared at 165 °C with corresponding values of 0.109 C/m^2 and 21.8 J/cm^3 (Fig. 8a.b). Since the U_e of dielectric materials is determined by both the field-induced polarization $P_{in\text{-}max}$ and the breakdown strength E_b, enhancing the breakdown strength is also important. The E_b of materials is statistical and strongly related to the film quality. The E_b of PVDF P&F films prepared at different temperatures was analysed and fitted using a Weibull distribution (Fig. 8c). All of the P&F films exhibited outstanding breakdown strength compared to other PVDF-based polymers (Fig. 8e) because of their enhanced Young's modulus (Fig. S1), which is regarded as a determinant factor in the dielectric breakdown of polymer-based materials [24,55]. The 140 °C P&F films displayed the highest E_b of 880 kV/mm, while the lowest E_b of 636 kV/mm was found for the 60 °C P&F films. The difference between the films could be ascribed to the higher film homogeneity arising from the repair of defects (e.g. microcracks, pores etc.) in the high temperature P&F films (≥140 °C) during each P&F cycle. Another contribution to the lower breakdown strength in the low temperature P&F film could be the early polarization saturation caused by the quick boost of $P_{in\text{-}max}$ at relatively low electric fields (Fig. 8d), which is prevalent in the terpolymer P(VDF-TrFE-CFE/CTFE) [17]. Therefore, combining both a high $P_{in\text{-}max}$ and E_b, an extremely high U_e of 39.8 J/cm^3, with an efficiency of 72.8%, was achieved at the E_b of

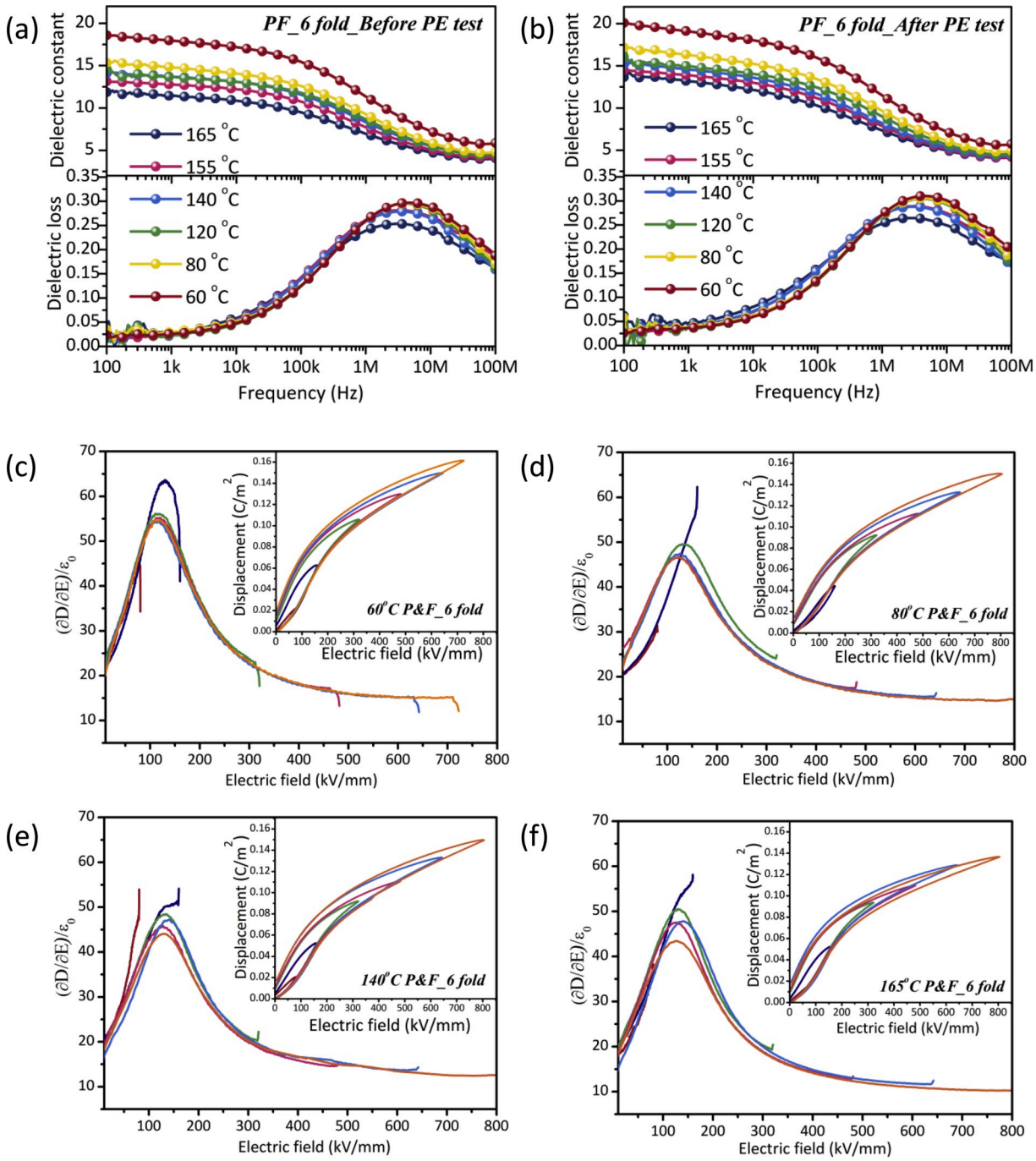

Fig. 7. Comparison of dielectric properties as a function of frequency for 6-fold P&F films prepared at 60 °C–165 °C: (a) before ferroelectric testing; and (b) after obtaining *D-E* loops at 400 kV/mm. The electric field dependence of $(\partial D/\partial E)/\varepsilon_0$ of charging process for 6-fold film P&F at: (c) 60 °C; (d) 80 °C; (e) 140 °C; and (f) 165 °C. Inset shows the corresponding unipolar *D-E* loops.

880kV/mm of the 140 °C P&F films. This is the highest U_e ever reported for any polymer-based materials (Fig. 8e).

4. Conclusions

We successfully fabricated free-standing PVDF homopolymer films with relaxor-like behaviour and a giant discharged energy density of 39.8 J/cm^3 at an ultrahigh E_b of 880 kV/mm, using the facile and scalable "press & folding" method, which is the best performance reported for any polymer-based material. By manipulating the P&F temperature, the film press-folded at 60 °C exhibited the highest U_e of 26.6 J/cm^3 at the same applied field of 640 kV/mm, indicating that a lower P&F temperature is more favourable for building up high internal lattice strain (~7.11%), which broadened the polymer interchain distance to 4.54 Å (4.24 Å for internal stress free β-PVDF) and enhanced the reversibility of the polar nanostructure of PVDF. Utilising internal stress to engineer polar nanostructures, materials with superior dielectric and energy storage properties were produced using the facile and scalable P&F technique. This new approach could produce a step change in the development of polymer dielectric energy storage materials.

Declaration of competing interest

The authors declare that they have no known competing financial

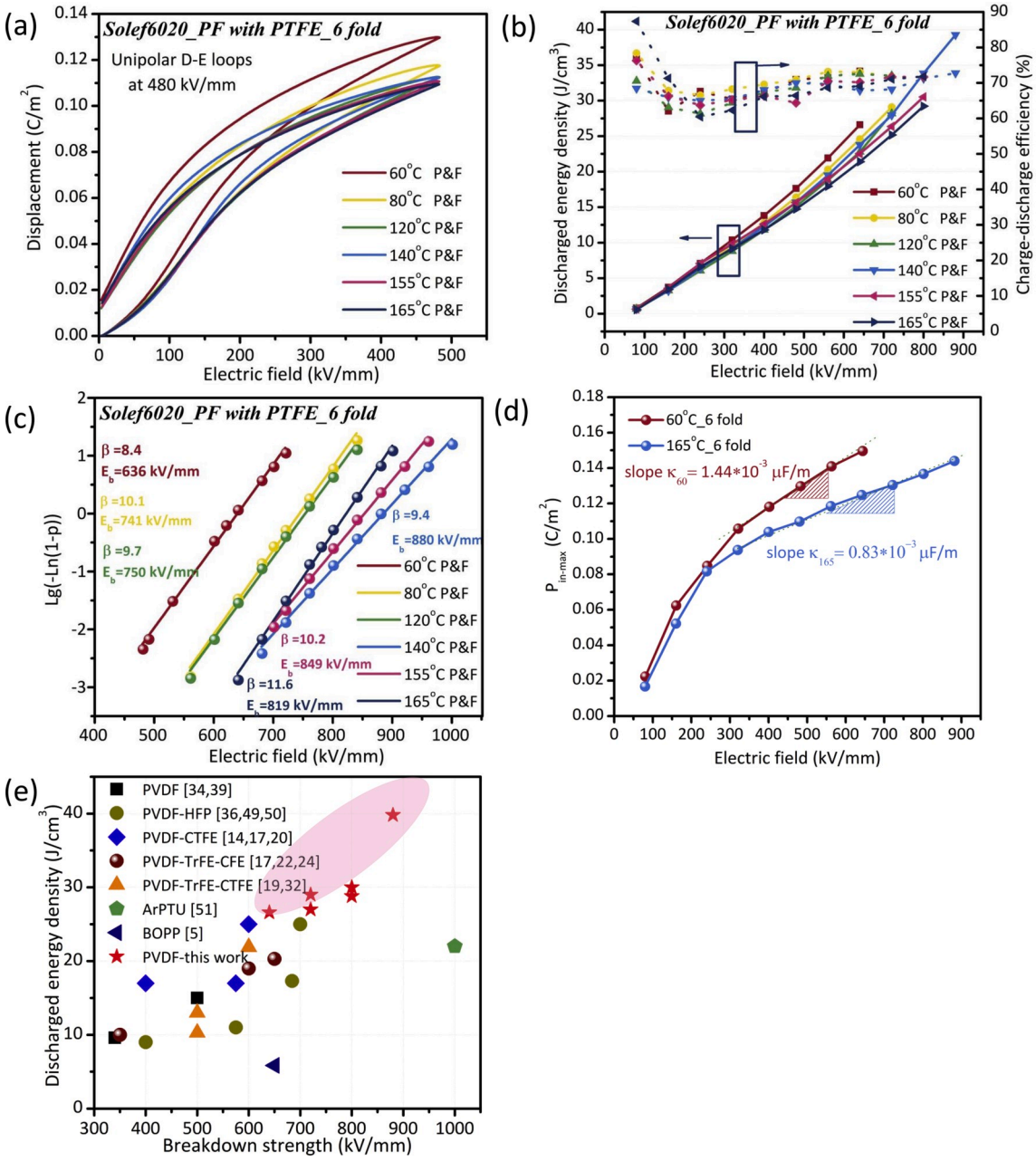

Fig. 8. (a) Unipolar *D-E* loops at 10 Hz; (b) discharged energy density and charge-discharge efficiency; (c) dielectric breakdown strength analysis using two-parameter Weibull distribution for films prepared at different processing temperatures. (d) Comparison of $P_{\text{in-max}}$ with increasing electric field for 6-fold films prepared at 60 and 165 °C. (e) Discharged energy density comparison of currently available polymers for dielectric energy storage applications [5,14,17–20,22,24,32,34,36,39,55–57].

interests or personal relationships that could have appeared to influence the work reported in this paper.

CRediT authorship contribution statement

Xintong Ren: Conceptualization, Methodology, Investigation, Data curation, Formal analysis, Writing - original draft. **Nan Meng:** Conceptualization, Methodology, Data curation, Writing - review & editing. **Han Zhang:** Methodology, Writing - review & editing. **Jiyue Wu:** Data curation, Writing - review & editing. **Isaac Abrahams:** Investigation, Data curation, Writing - review & editing. **Haixue Yan:** Methodology, Writing - review & editing. **Emiliano Bilotti:** Conceptualization, Supervision, Writing - review & editing. **Michael John Reece:** Conceptualization, Methodology, Supervision, Writing - review & editing.

Acknowledgements

This work was supported by the Engineering and Physical Sciences Research Council [EP/L017695/1, MASSIVE]. Xintong Ren (CSC No.: 201606280030) and Jiyue Wu (CSC No.: 201506630005) would like to thank the China Scholarship Council for the financial support.

Appendix A. Supplementary data

Supplementary data to this article can be found online at https://doi.org/10.1016/j.nanoen.2020.104662.

References

[1] X. Hao, J. Adv. Dielectr (2013) 1330001, 03.
[2] Prateek, V.K. Thakur, R.K. Gupta, Chem. Rev. 116 (2016) 4260–4317.
[3] B. Dunn, H. Kamath, J.-M. Tarascon, Science 334 (2011) 928–935.
[4] C. Liu, Z. Yu, D. Neff, A. Zhamu, B.Z. Jang, Nano Lett. 10 (2010) 4863–4868.
[5] Y. Zhao, Q. Li, X. Zhang, H. Li, J. Lu, Z. Zhang, Macromol. Chem. Phys. 219 (2018) 1700621.
[6] E.J. Barshaw, J. White, M.J. Chait, J.B. Cornette, J. Bustamante, F. Folli, D. Biltchick, G. Borelli, G. Picci, M. Rabuffi, IEEE Trans. Magn. 43 (2007) 223–225.
[7] T. Christen, M.W. Carlen, J. Power Sources 91 (2000) 210–216.
[8] Z.-M. Dang, J.-K. Yuan, S.-H. Yao, R.-J. Liao, Adv. Mater. 25 (2013) 6334–6365.
[9] X. Wang, X. Lu, B. Liu, D. Chen, Y. Tong, G. Shen, Adv. Mater. 26 (2014) 4763–4782.
[10] R. Hasegawa, M. Kobayashi, H. Tadokoro, Polym. J. 3 (1972) 591–599.
[11] G.T. Davis, J.E. McKinney, M.G. Broadhurst, S.C. Roth, J. Appl. Phys. 49 (1978) 4998–5002.
[12] A.J. Lovinger, Science 220 (1983) 1115–1121.
[13] S. Wu, M. Lin, S.G. Lu, L. Zhu, Q.M. Zhang, Appl. Phys. Lett. 99 (2011) 132901.
[14] P. Khanchaitit, K. Han, M.R. Gadinski, Q. Li, Q. Wang, Nat. Commun. 4 (2013) 2845.
[15] J. Li, S. Tan, S. Ding, H. Li, L. Yang, Z. Zhang, J. Mater. Chem. 22 (2012) 23468–23476.
[16] F. Guan, J. Wang, L. Yang, J.-K. Tseng, K. Han, Q. Wang, L. Zhu, Macromolecules 44 (2011) 2190–2199.
[17] B. Chu, X. Zhou, K. Ren, B. Neese, M. Lin, Q. Wang, F. Bauer, Q.M. Zhang, Science 313 (2006) 334–336.
[18] B. Chu, X. Zhou, B. Neese, Q. Zhang, F. Bauer, ITDEI 13 (2006) 1162–1169.
[19] Z. Zhang, Q. Meng, T.C.M. Chung, Polymer 50 (2009) 707–715.
[20] X. Zhou, B. Chu, B. Neese, M. Lin, Q.M. Zhang, ITDEI 14 (2007) 1133–1138.
[21] Q.M. Zhang, V. Bharti, X. Zhao, Science 280 (1998) 2101–2104.
[22] X. Zhang, Y. Shen, Z. Shen, J. Jiang, L. Chen, C.-W. Nan, ACS Appl. Mater. Interfaces 8 (2016) 27236–27242.
[23] M. Rahimabady, K. Yao, S. Arabnejad, L. Lu, V.P. Shim, D. Cheong Wun Chet, Appl. Phys. Lett. 100 (2012) 252907.
[24] Q. Li, G. Zhang, F. Liu, K. Han, M.R. Gadinski, C. Xiong, Q. Wang, Energy Environ. Sci. 8 (2015) 922–931.
[25] Y. Wang, J. Cui, Q. Yuan, Y. Niu, Y. Bai, H. Wang, Adv. Mater. 27 (2015) 6658–6663.
[26] H. Tang, Y. Lin, H.A. Sodano, Adv. Energy Mater. 3 (2013) 451–456.
[27] K. Bi, M. Bi, Y. Hao, W. Luo, Z. Cai, X. Wang, Y. Huang, Nano Energy 51 (2018) 513–523.
[28] Y. Zhang, C. Zhang, Y. Feng, T. Zhang, Q. Chen, Q. Chi, L. Liu, G. Li, Y. Cui, X. Wang, Z. Dang, Q. Lei, Nano Energy 56 (2019) 138–150.
[29] J. Chen, Y. Wang, Q. Yuan, X. Xu, Y. Niu, Q. Wang, H. Wang, Nano Energy 54 (2018) 288–296.
[30] J. Jiang, Z. Shen, J. Qian, Z. Dan, M. Guo, Y. He, Y. Lin, C.-W. Nan, L. Chen, Y. Shen, Nano Energy 62 (2019) 220–229.
[31] B. Xie, Q. Zhang, L. Zhang, Y. Zhu, X. Guo, P. Fan, H. Zhang, Nano Energy 54 (2018) 437–446.
[32] Z. Zhang, T.C.M. Chung, Macromolecules 40 (2007) 783–785.
[33] X. Ren, N. Meng, H. Yan, E. Bilotti, M.J. Reece, Polymer 168 (2019) 246–254.
[34] W. Li, Q. Meng, Y. Zheng, Z. Zhang, W. Xia, Z. Xu, Appl. Phys. Lett. 96 (2010) 192905.
[35] N. Meng, X. Zhu, R. Mao, M.J. Reece, E. Bilotti, J. Mater. Chem. C 5 (2017) 3296–3305.
[36] F. Guan, J. Pan, J. Wang, Q. Wang, L. Zhu, Macromolecules 43 (2009) 384–392.
[37] F. Guan, J. Wang, J. Pan, Q. Wang, L. Zhu, Macromolecules 43 (2010) 6739–6748.
[38] L. Yang, J. Ho, E. Allahyarov, R. Mu, L. Zhu, ACS Appl. Mater. Interfaces 7 (2015) 19894–19905.
[39] Y. Wang, J. Cui, L. Wang, Q. Yuan, Y. Niu, J. Chen, Q. Wang, H. Wang, J. Mater. Chem. A 5 (2017) 4710–4718.
[40] N. Meng, X. Ren, G. Santagiuliana, L. Ventura, H. Zhang, J. Wu, H. Yan, M.J. Reece, E. Bilotti, Nat. Commun. 10 (2019) 4535.
[41] M. Ree, C.W. Chu, M.J. Goldberg, J. Appl. Phys. 75 (1994) 1410–1419.
[42] S.R. Oh, K. Yao, C.L. Chow, F.E.H. Tay, Thin Solid Films 519 (2010) 1441–1444.
[43] V. Bhavanasi, V. Kumar, K. Parida, J. Wang, P.S. Lee, ACS Appl. Mater. Interfaces 8 (2015) 521–529.
[44] S. Shen, A. Henry, J. Tong, R. Zheng, G. Chen, Nat. Nanotechnol. 5 (2010) 251.
[45] J. Gregorio, Rinaldo, M. Cestari, J. Polym. Sci., Part B: Polym. Phys. 32 (1994) 859–870.
[46] T. Furukawa, J.X. Wen, K. Suzuki, Y. Takashina, M. Date, J. Appl. Phys. 56 (1984) 829–834.
[47] H. Yan, F. Inam, G. Viola, H. Ning, H. Zhang, Q. Jiang, T. Zeng, Z. Gao, M.J. Reece, J. Adv. Dielectr (2011) 107–118, 01.
[48] C. Wan, C.R. Bowen, J. Mater. Chem. A 5 (2017) 3091–3128.
[49] C. Song, L. Du, L. Qi, Y. Li, X. Li, Y. Li, JMiMi 27 (2017) 105014.
[50] Y. Oka, N. Koizumi, Jpn. J. Appl. Phys. 24 (1985) 669–673.
[51] K. Tashiro, Y. Itoh, M. Kobayashi, H. Tadokoro, Macromolecules 18 (1985) 2600–2606.
[52] H. Ohigashi, K. Koga, Jpn. J. Appl. Phys. 21 (1982) L455.
[53] T. Furukawa, PTMJ 18 (1989) 143–211.
[54] J. Jiang, X. Zhang, Z. Dan, J. Ma, Y. Lin, M. Li, C.-W. Nan, Y. Shen, ACS Appl. Mater. Interfaces 9 (2017) 29717–29731.
[55] X. Zhou, X. Zhao, Z. Suo, C. Zou, J. Runt, S. Liu, S. Zhang, Q.M. Zhang, Appl. Phys. Lett. 94 (2009) 162901.
[56] X. Zhang, Y. Shen, B. Xu, Q. Zhang, L. Gu, J. Jiang, J. Ma, Y. Lin, C.-W. Nan, Adv. Mater. 28 (2016) 2055–2061.
[57] S. Wu, W. Li, M. Lin, Q. Burlingame, Q. Chen, A. Payzant, K. Xiao, Q.M. Zhang, Adv. Mater. 25 (2013) 1734–1738.

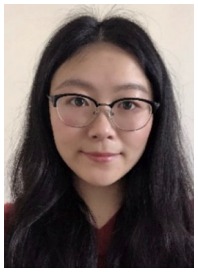

Xintong Ren is a currently a Ph.D. candidate at Queen Mary University of London (QMUL), UK. She received her B.Eng. degree in Electronics & Information Engineering from Northwestern Polytechnical University (NWPU), Xi'an, China. Her research focuses on electroactive polymers for dielectric energy storage applications, including novel processing approaches and investigating the relationships between structures and dielectric/ferroelectric properties.

Dr. Nan Meng received her B.Eng. degree from College of Materials Science and Engineering, Donghua University (DHU), Shanghai, China, and completed her Ph.D. in Materials Science and Engineering, Queen Mary University of London in 2017. Currently she is working as a postdoctoral fellow in the group of Dr. Emiliano Bilotti, where her research is focused on the development of polymer based dielectric capacitors for high power energy storage applications.

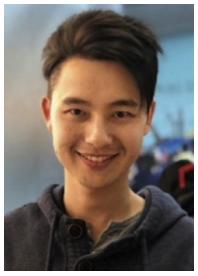

Dr. Han Zhang is a Lecturer in Materials Science at Queen Mary University of London (QMUL) and heads the Composites research group at QMUL. He obtained his BEng from Beihang University (formerly known as BUAA) and Ph.D. from QMUL. His research focuses mainly on multifunctional composites, smart materials, hierarchical lightweight composites and nanomaterials, with innovations from materials processing to final applications. Han has extensive experience from design and processing to advanced characterisations and interpretation of polymer and composite materials, with more than 40 publications in peer-reviewed journals and book chapters.

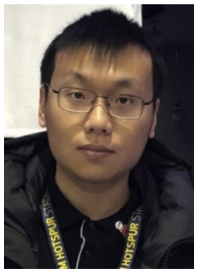

Dr. Jiyue Wu is currently a postdoctoral researcher at Uppsala University, Sweden. He received his Ph.D. degree in Materials Science at Queen Mary University of London (QMUL) in 2019. His research interest covers the synthesis of advanced dielectric and piezoelectric materials for energy storage and actuator applications, and the development of nanoscale electronic biosensors for clinical applications.

Dr. Isaac Abrahams is a Senior Lecturer in Inorganic Chemistry in the School of Biological and Chemical Sciences at Queen Mary University of London (QMUL), where he is Deputy Head of the Department of Chemistry. In the 27 years he has been at QMUL, his research has been focused on exploring the structure property relationships in a variety of energy materials including electrolytes and cathode for batteries and fuel cells, as well as ferroelectrics for energy storage devices.

Dr. Haixue Yan is a Senior Lecturer in Materials at the School of Engineering and Materials Science in Queen Mary University of London (QMUL). He received his Ph.D. in Materials Science and Technology from Shanghai Institute of Ceramics, Chinese Academy of Sciences in 2001. Since that, he joined QMUL as an academic visitor and research assistant. At QMUL, he was appointed as an Academic Fellow in 2011 and Senior Lecturer in 2015. His research area includes processing and analysis of the microstructures and properties of advanced materials including dielectrics, ferroelectrics, thermoelectrics, ceramic-carbon composites and dental materials.

Dr. Emiliano Bilotti is a Reader in School of Engineering and Materials Science at Queen Mary University of London (QMUL), UK. He joined QMUL for his Ph.D. study on polymer/clay nanocomposites and new environmentally friendly flame retardant materials in 2004. His research interests lie in Processing-Structure-Property relationships in polymeric materials. He has extensive experience in processing and characterisation of polymer nanocomposites and smart polymers. More recently, his research has focused on flexible self-regulating heating devices (pyro-resistive materials) and polymers for energy (organic thermoelectrics, ferroelectric, piezoelectric).

Dr. Michael J. Reece is a Professor in the School of Engineering and Materials Science at Queen Mary University of London (QMUL), UK. His current research focuses on the development of field (electric, magnetic and gravity) assisted processing to produce nanostructured, textured, hierarchical and non-equilibrium functional ceramics, including thermoelectrics, ferroelectrics and high entropy ceramics. He is also interested in the development of dielectric materials for energy storage applications.